Statistical Spectral Fitting of Potential Brown Dwarf Binary Systems

Leanne T. Farnbach

A senior thesis submitted to the faculty of
Brigham Young University
in partial fulfillment of the requirements for the degree of

Bachelor of Science

Denise Stephens, Advisor

Department of Physics and Astronomy

Brigham Young University

April 2017

ABSTRACT

Statistical Spectral Fitting of Potential Brown Dwarf Binary Systems

Leanne T. Farnbach
Department of Physics and Astronomy, BYU
Bachelor of Science

Brown dwarf binary systems are typically too small and cold to be visually resolved, making the study of their spectral features the next best method to determine the general nature of these particular systems. I obtained data from the Spitzer Heritage Archive in the near to mid-infrared spectrum for several brown dwarf binary candidates. Using a least-squares approach and over a thousand synthetic spectral models, I performed a statistical analysis to determine which models best fit the original data. From these models, I determined the most likely parameter values for each component of either the single or binary system which include the temperature, surface gravity, cloud density, and the amount of atmospheric convection for each star. A binary system, or combination of two models, was found to better fit the following dwarfs: Kelu-1, 2MASSW J0036159+182110, 2MASSW J2224438-015852, SDSS J080531.83+481233.1, SDSS J105213.51+442255.7AB, and 2MASS J05591914-1404488. Kelu-1 and SD1052 are visually confirmed binary systems. The results of the statistical fitting match the known temperatures of each component for both stars, implying that this is a reliable method. The next step will be to identify and perform the statistical spectral analysis on additional brown dwarf binary candidates.

Keywords: Kelu-1, 2MASSW J0036159+182110, 2MASSW J2224438-015852,
SDSS J080531.83+481233.1, SDSS J105213.51+442255.7AB, 2MASS J05591914-1404488,
brown dwarf binary, spectral fitting, least squares

ACKNOWLEDGMENTS

This research has made use of the NASA/IPAC Infrared Science Archive, which is operated by the Jet Propulsion Laboratory and California Institute of Technology, under contract with the National Aeronautics and Space Administration. The IRS was a collaborative venture between Cornell University and BAll Aerospace Corporation funded by NASA through the Jet Propulsion Laboratory and Ames Research Center.

I give my thanks to Dr. Denise Stephens for her instruction and support, and Dr. Tom Stephens for writing the code used in the statistical fitting.

My gratitude goes to Riley Finnegan and Baylee Danz for providing the potential binary candidates for this paper. I would also like to acknowledge the BYU REU program for this research opportunity, and the BYU ORCA, BYU RA, and National Science Foundation for their funding (NSF-1461219).

Last, I would like to thank my husband, Hans Farnbach, for his patience in reading and editing numerous drafts.

Contents

List of Figures

List of Tables

Chapter 1

Introduction

1.1 Brown Dwarfs

Brown dwarfs are an intermediary between stars and planets, whose size and atmosphere resemble "Super-Jupiters" (i.e., gas planets in the universe that are similar to, but much larger than, our own Jupiter). The main difference between these and other stars like our sun is that brown dwarfs are too small to sustain hydrogen fusion, as there is not enough gravitational pressure to maintain high temperatures in the core. On the other hand, brown dwarfs are not classified as planets because they form, like all other stars, inside dense molecular clouds (see Figure 1.1). Planets, like those in our solar system, are instead born as materials begin to clump together in the accretion disk and clear their orbits around a central star. It is difficult to be certain of the origin of a suspected brown dwarf, as going back in time and witnessing the formation thereof is currently impossible. Instead, brown dwarfs are classified by analyzing their temperature and spectral features.

Stars are given letter classifications based on their temperatures. Blue giants, or O stars, are the hottest category with temperatures around 40 000 Kelvin (K), while Y dwarfs are the coldest at 300K. From hot giants to cold dwarfs, the temperature sequence order is: O, B, A, F, G, K, M, L, T,

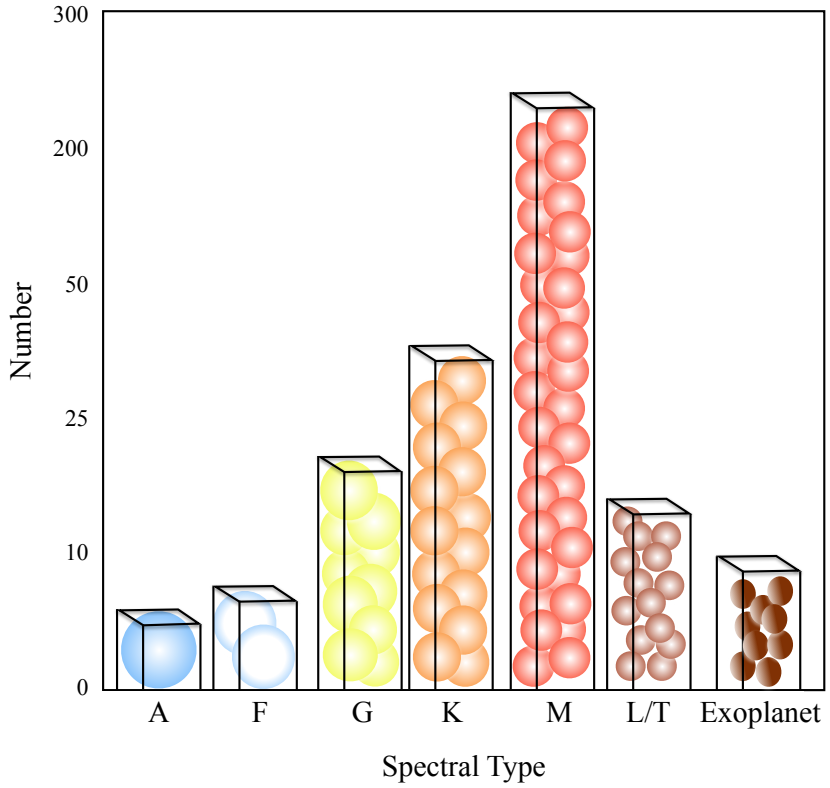

Figure 1.1 Spectral type, or temperature, of stars compared to the number that have been detected. The relationship between number and spectral type indicates that colder stars are the most abundant in the Universe. Brown dwarfs and exoplanets appear to be the exception, but this is most likely due to the fact that these small, faint objects are difficult to detect.

Y. Stars that begin their lives as M dwarfs, the warmest of the brown dwarf family, will eventually cool and become Y brown dwarfs.

Brown dwarfs are difficult to detect and study due to their cold temperature and small size. While there are currently a limited number of brown dwarfs that can be studied, observations of all spectral types of stars indicate that brown dwarfs should be the most common type of star in the Universe. Blue giants (O, B, and A stars) are the rarest objects, with the detected number of each type of star increasing as the temperature decreases (Figure 1.1). As advancements in telescopes are made, it is suspected that hundreds of additional brown dwarfs will be found, making the study of these abundant stars crucial in understanding the life and evolution of stars.

I analyzed the spectral features of only two types of brown dwarfs for this paper, these types being L and T (see Figure 1.2). L dwarfs range in temperature from 1300-2250K and contain iron hydride (FeH) and carbon monoxide (CO) in their atmospheres (Mamajek 2017). As L dwarfs cool, they evolve into T dwarfs with temperatures as low as 500K. In this stage, the CO molecules split and bond with hydrogen to form water (H_2O) and methane (CH_4).

The way that different molecules interact with each other and the layers of the atmosphere they occupy can affect the shape of the spectral features (Esplin 2010). These are a result of many factors that are difficult to determine, such as the age and mass of a particular star. For example, a low-mass L brown dwarf can exhibit the same spectral features as a high-mass T dwarf (Esplin 2010). The only way to calculate the masses of brown dwarfs is by analyzing the orbital parameters of binary systems. More than half of all stars are members of a binary system, and naturally formed binaries are often made up of objects that have the same relative age and composition. Studying brown dwarf binary systems and their observed spectra leads to a greater understanding of the relationship between temperature, surface gravity, and atmospheric properties of all brown dwarfs.

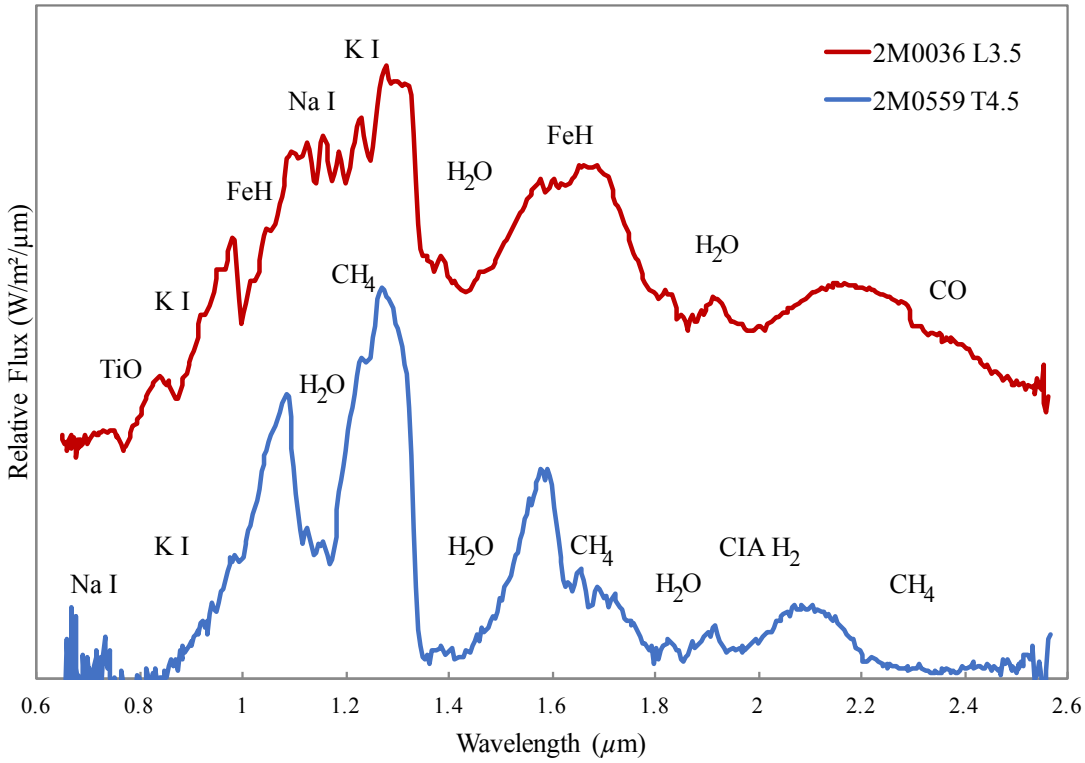

Figure 1.2 L (red) and T (blue) dwarf spectra in the infrared. L dwarfs are the warmer of the two classifications. The top spectral line shows that iron hydride (FeH) is present. At the bottom, T dwarfs have strong methane (CH_4) and water (H_2O) absorption lines as well as broadened sodium (Na) and potassium (K) lines. This figure is similar to that of Burgasser (2003), with spectral data from Burgasser *et al.* (2006) and Chiu *et al.* (2006).

1.2 Previous Work at BYU

Stephens *et al.* (2009) performed a statistical spectral analysis on 21 L and T brown dwarfs that were observed with the Spitzer Space Telescope (Werner et al. 2004). They used 600 model spectra provided by Saumon and Marley (2008) to analyze the temperature, surface gravity, cloudiness, and atmospheric mixing parameters of each brown dwarf. These models will be discussed further in Chapter 3. For the best single fit, each model is compared to the original spectra and a list of the best matched spectra is returned. The binary fitting process is much longer, as two model spectra are added together and compared with the original data, which is repeated for every possible model combination. Only four out of the 21 targets were found to potentially be binary systems based on the results of their best statistical fit, these being 2MASSW J0036159+182110 (2M0036), SDSS J080531.83+481233.1 (SD0805), SDSS J105213.51+442255.7AB (SD1052AB), and 2MASS J05591914-1404488 (2M0559). The best single and binary parameters for these four, as well as 2MASSW J2224438-015852 (2M2224), are shown in Figure 1.3. The single and binary model spectra results were too similar to statistically determine if any of the five mentioned objects is in a binary system.

Esplin (2010) used the methods and results of Stephens *et al.* (2009) to perform a detailed study on the possible binary 2M0559. As there had been an upgrade to the software used by Stephens *et al.* (2009), Esplin (2010) made the necessary corrections to the procedures and wrote several programs to perform the analysis. Esplin was able to improve upon the results of Stephens *et al.* (2009) for the dwarf 2M0559, and showed that, statistically, the star is likely an unequal temperature binary system (see Figure 1.4).

During the summer of 2016, Riley Finnegan and Bailey Danz identified several brown dwarf binary candidates based on a point-spread function (PSF) fitting technique. They downloaded visible observations from the Hubble Space Telescope for several brown dwarfs. Tiny Tim, a program that models the spread of light across the lens, was used to create point-spread functions

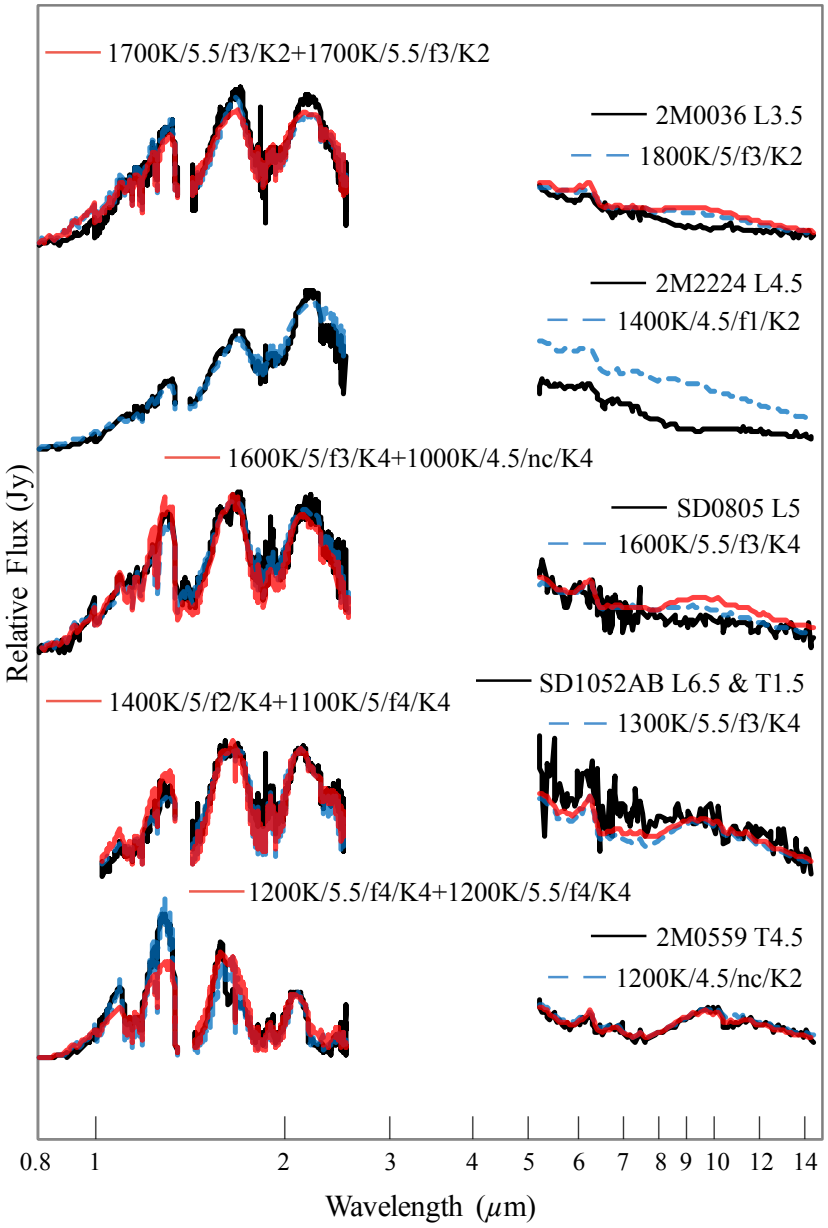

Figure 1.3 Recreation of the best single and binary results from Stephens *et al.* (2009) for 2M2224, 2M0036, SD0805, known binary SD1052AB, and 2M0559. The observed spectra for each is shown in black, while the best single (blue, dashed lines) and binary (red lines) fits are also indicated. The naming scheme for each fit is a list of parameters in the following order: temperature, surface gravity, cloud density, and vertical mixing (explained further in Chapter 3). The above best parameters were chosen by inspection rather than statistics.

in order to subtract the light from possible primary objects in order to reveal a secondary one (Krist & Hook 2004). The last step involved running a single and binary fitting program on the residuals, which calculated possible magnitude combinations. They recorded several possible brown dwarf binary candidates based on the returned magnitudes, but only six brown dwarfs had sufficient spectral data in order to perform a statistical fitting analysis (see Table 1.1). Five of the six have previously been studied by Stephens *et al.* (2009) (see Figure 1.3) and Esplin (2010).

In this thesis, I used and improved upon Esplin's methods from 2010, and present the best single and binary fitting results for Kelu-1, 2M0036, 2M2224, SD0805, SD1052AB, and 2M0559. Kelu-1 and SD1052AB are both visually resolved, confirmed binary systems that were used to test the reliability of these results.

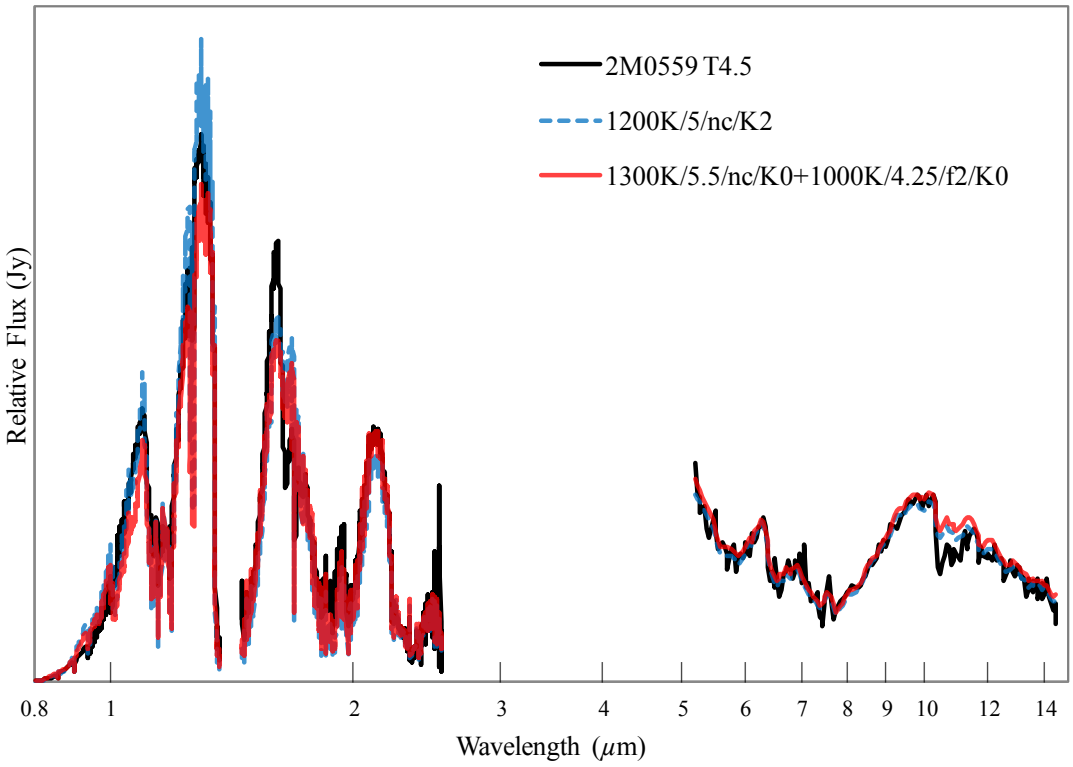

Figure 1.4 Recreation of the best single and binary results for 2M0559 from Esplin (2010). The best single (blue, dashed line) and binary (red line) model fits were chosen statistically. The binary result better fits the observed spectra (black line) than the models chosen by Stephens *et al.* (2009) for the same object.

Table 1.1 Brown Dwarfs with Spectra from 0.8-14.5μm

Name	Spectral Type	Temperature	Binary	Notes
Kelu-1	L3.5 & L2	1770-1960K	yes	1, 2, 3, 4
2MASSW J0036159+182110	L3.5	1770K	...	3, 5, 6
2MASSW J2224438-015852	L4.5	1650K	...	3, 7, 8
SDSS J080531.83+481233.1	L5	1590K	...	7, 9, 10
SDSS J105213.51+442255.7AB	T1.5 & L6.5	1220-1450K	yes	11, 12, 13
2MASS J05591914-1404488	T4.5	1090K	...	3, 14, 15

Note. – All temperatures provided by Mamajek (2017). (1) Discovered by Ruiz *et al.* (1997); (2) near-infrared data provided by Ruiz *et al.* (1997) and Leggett *et al.* (2001); (3) mid-infrared data requested by Houck *et al.* (2004); (4) resolved binary by Liu and Leggett (2005); (5) discovery by Reid *et al.* (2000); (6) near-infrared data provided by Reid *et al.* (2001), reflux-calibrated by Leggett *et al.* (2002); (7) discovery by Kirkpatrick *et al.* (2000); (8) near infrared data provided by Kirkpatrick *et al.* (2000), Geballe *et al.* (2002), Knapp *et al.* (2004); (9) near infrared data provided by Knapp *et al.* (2004), Chiu *et al.* (2006); (10) mid-infrared data requested by Sandy Leggett in 2004 (Program ID 3431); (11) discovery and near-infrared data by Chiu *et al.* (2006); (12) mid-infrared data requested by David Golimowski in 2006 (Program ID 20514); (13) resolved L and T binary by Dupuy *et al.* (2015); (14) discovery by Burgasser *et al.* (2000a); (15) near-infrared data provided by Leggett *et al.* (2002), Geballe *et al.* (2002), Burgasser *et al.* (2003).

Chapter 2

Observations

Mid-infrared spectral data was obtained from the Spitzer Space Telescope for each brown dwarf that will be analyzed in Chapter 4. The images obtained required a detailed cleaning and extraction process before being combined with published near-infrared data.

2.1 Data Acquisition

The spectral observations were made with the Spitzer Infrared Spectrograph (IRS) on Staring Mode (Houck et al. 2004). The image cleaning and extraction process used only three types of files, all of which were processed and partially reduced by the Infrared Science Archive. The exposure-level data frames, or bcd files, contain the spectrum that was extracted. Func files contain the uncertainty levels for the pixels in the bcd images and bmask files contain uncertainty values which are used to remove known impurities (Dyk et al. 2013).

The bcd images are the result of starlight passing through the diffraction grating on the spectrograph, and contain three spectral orders (see Figure 2.1). The first order records wavelengths from 7.57-14.28μm, while the second order contains values from 5.21-7.56μm. The third order was not used in the extraction and analysis, but includes wavelengths from 14.29-20.66μm (Dyk et al.

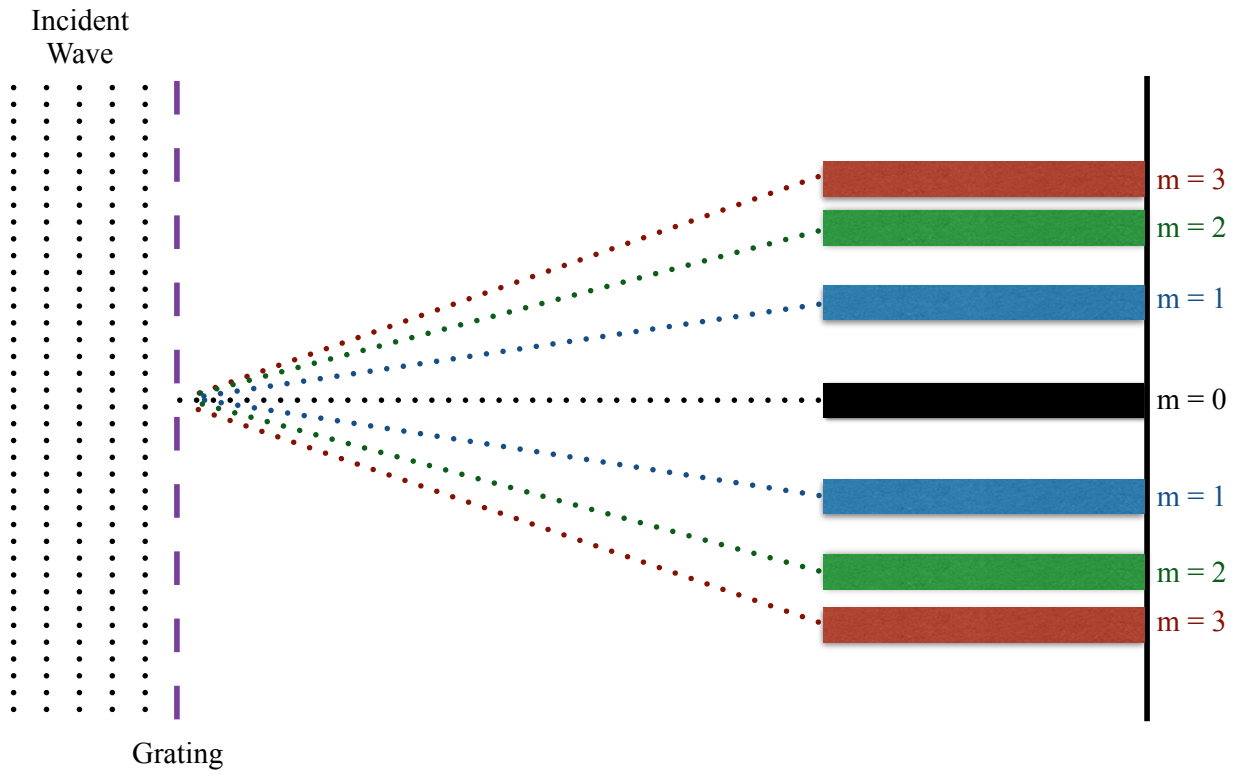

Figure 2.1 Example of a diffraction grating on a spectrograph that results in four beams, or orders, with $m = 0$ being the incident beam. A diffraction grating is made up of closely spaced slits. When light strikes the grating, the different wavelengths that make up the incident light are separated. Each wavelength of light diffracts at a different angle. The more narrow and numerous the slits, the higher the resolution of the observed spectra.

2013). Near-infrared data from 0.8-2.5μm was also obtained and combined with the extracted spectra (See Table 1.1, Notes). Spectral data was obtained from two different positions in the slit (Figure 2.2).

2.2 Reduction Procedures

The white lines that indicate the first, second and third orders in Figure 2.2 contain small fluctuations in light. To obtain the spectral features from each of these images, the images were cleaned to remove bad pixels in order for the correct flux values of each line to be extracted and plotted.

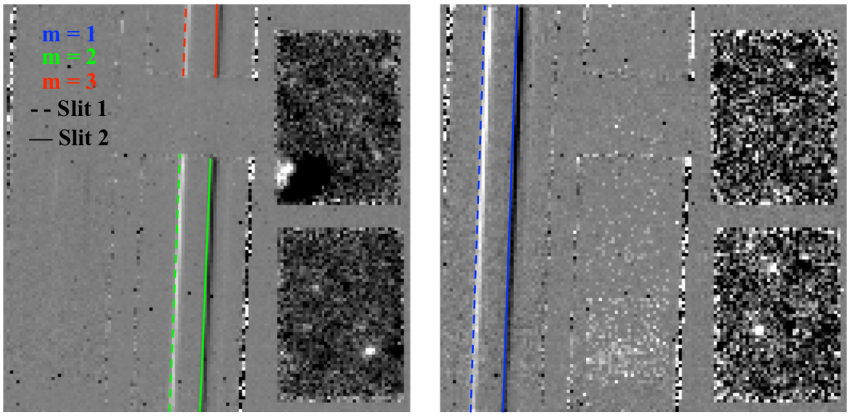

Figure 2.2 The reduced images shown were taken with the Spitzer Infrared Spectrograph. The white lines occupying slit position 1 are where the flux values, or spectral lines of the observed star, are stored. The black lines indicate slit position 2, which was not used in these particular images. On the left image, order 2 is indicated by the green lines. Order 3 is shown by the red lines near the top. The image on the right shows order 1 (blue lines). The two boxes containing black pixels and the line closest to them are for direct imaging, but were not used in this analysis.

The first step in preparing the Spitzer bcd images for spectral extraction involves identifying and recording bad pixels on each frame. Two types of bad pixels that require attention are dead pixels and hot pixels. Dead pixels can be found in the same position on every image, and are thus relatively simple to identify. Hot pixels, on the other hand, can vary in frame and location because they appear when the camera sensor becomes hot during long exposures and thereby record false values. The Image Reduction and Analysis Facility (IRAF) program found these unstable pixels on each of the bcd frames and recorded the pixel values with their X-Y coordinates on the frame (Tody 1986). A MATLAB code created by Esplin (2010) was used to create mask files which record dead and hot pixel values for each image. Flagged pixels were labeled as acceptable if the value of the pixel was within five times the standard deviation of the median of all surrounding pixels. Mask files contained a list of the locations of the bad pixels and their surrounding median values.

The dead and zero-value pixels were removed from the bcd images, and they were replaced

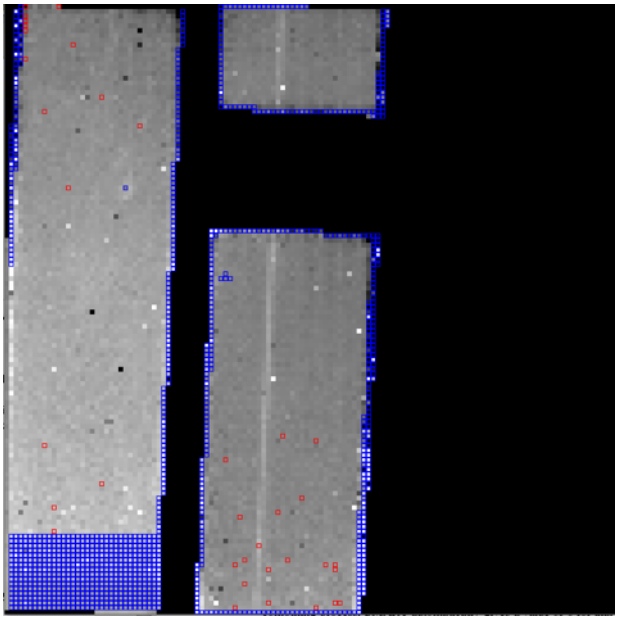

Figure 2.3 Example of a combined image mask in IRSClean. Bad pixels outlined in red were identified by the mask file from the code written by Esplin (2010), while pixels in blue were identified and labeled by the program IRSClean.

with the median values recorded in the mask files. This was facilitated by the use of a general mask file, created by combining the mask files of each slit position. The text files were then converted into an image format in IRAF. The resulting images were uploaded into a program within the Spectroscopic Modeling Analysis and Reduction Tool (SMART) called IRSClean to create additional bad pixel masks from the Spitzer bcd, func, and bmask image files (Lebouteiller et al. 2009; Higdon et al. 2004). All masks were combined and the bad pixels were removed from each bcd, func, and bmask image (Figure 2.3).

The final step in reduction used the SMART program for final cleaning and extraction. First, the cleaned uncertainty and bmask files were combined with each corresponding bcd image. The individual exposures were then merged to create one image file for each slit position. These images, known as sky images, were used to eliminate the background radiation and were subtracted from each other, depending on the order and slit position. Order 2, position 1 sky images subtract off

order 2, position 2 sky images and vice versa. This subtraction is the single most important step in reducing the data, as it removes background emission and low-level rogue pixels, leaving behind a clearly identifiable spectral line.

An optimal extraction was then performed on the sky subtracted images, which included a flux calibration (Figure 2.4). Each pixel on the charge-coupled device (CCD) within the spectrometer reacts differently to the light received, and these responses can change over time. The flux calibration performed by SMART corrects this problem by using spectra from the stars HR6348, HD173511, and HR7341 that are obtained by the Spitzer Telescope every few days. The images from these stars become the Relative Spectral Response Functions (RSRF) that the program uses as calibration standards to account for pixel sensitivity (Esplin 2010).

Finally, spectra were extracted from each position in both orders and merged them together to create a spectrum that spans from 5 to 14μm with flux values in Jansky (Jy), which was exported into a text file. Near-infrared data from 0.8-2.5μm was converted into units of Jy and combined with the extracted data to create a final spectrum ready for analysis.

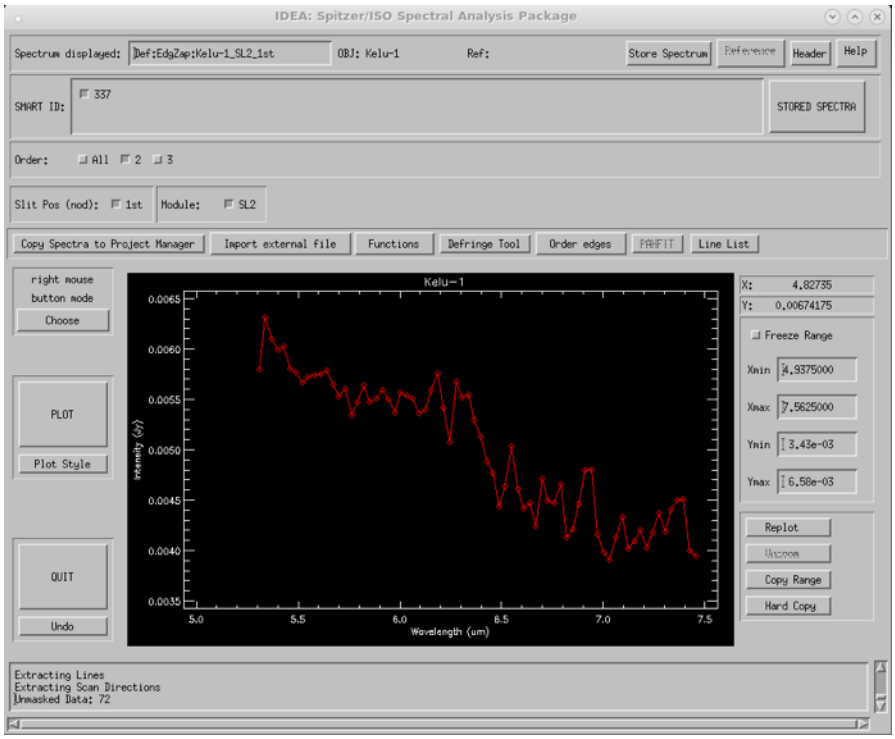

Figure 2.4 Screenshot of the extraction window inside of SMART. This shows the extracted spectra for the object Kelu-1, from order 2, slit position 1.

Chapter 3

Statistical Modeling

Synthetic brown dwarf models were obtained from two published sources, with each model being identified by a specific temperature, surface gravity, cloud density, and atmospheric convection. The models were modified to match the spectral resolution of the observed brown dwarf data, and the single and binary fitting equations are described.

3.1 Models and Parameters

Over a thousand brown dwarf models were created by Saumon and Marley (2008) and Morley *et al.* (2012) by using permutations of the temperature, gravity, cloud, and vertical mixing parameters. Each model spectrum is associated with a specific temperature (T_{eff}) which spans from 500-2400K in increments of 100K. The absorption features in spectra are highly temperature-dependent, as certain molecules are more abundant on L dwarfs than on T, and vice versa. For this reason, the temperature is the most influential parameter out of the four that are used.

The surface gravity, cloud, and convection parameters each impact the model spectra in small, but different, ways. Surface gravity affects the width of the absorption lines. High surface gravity values lead to pressure broadening, or a widening of the absorption features. The log(g) values

range from 4-5.5, with surface gravity (g) being in cm/s^2.

The cloud parameter (f_{sed}) indicates the particle density of the clouds. According to Cooper *et al.* (2003), this parameter contributes to several effects that alter the spectral features. A significant amount of clouds can lead to condensation and rain in the upper atmosphere, which depletes the upper atmosphere of some condensates. Thick clouds can also smooth out spectral features, block out surface light, and lead to a greenhouse effect that warms the atmosphere. The models vary in cloud presence on a scale from 0-5 with 0 being no cloud cover (nc), 1 being optically thick, and 5 being optically thin cloud cover.

The final parameter is vertical mixing (K_{zz}), or convection in the atmosphere. The values range from 0 (no mixing) to 6 (high mixing). This parameter mainly affects the strength of certain absorption features. For example, in a high vertical mixing system, NH_3 and CH_4 absorption bands are weaker because these molecules are pulled low into the atmosphere. From there, they are converted into N_2 and CO due to higher temperatures (Esplin 2010). While temperature may be the leading parameter in the overall shape of a brown dwarf spectra, the convection features combined with the cloud cover and density can have a large impact.

3.2 Preparing the Models

The spectral models from Saumon and Marley (2008) and Morley *et al.* (2012) were of a very high resolution as they were made computationally rather than by observation. In contrast, the observations made by the Spitzer Space Telescope led to spectra of a much lower resolution. Because of this, the models had to be smoothed to the same resolution as the extracted spectra (Figure 3.1). A spectrometer can only resolve a certain number of spectral peaks, as resolving power is directly related to the width of wavelengths covered by each pixel on the CCD (Esplin 2010). For example, suppose the spectrometer has a wavelength range of $\lambda = 20$ nanometers (nm) with a spectral

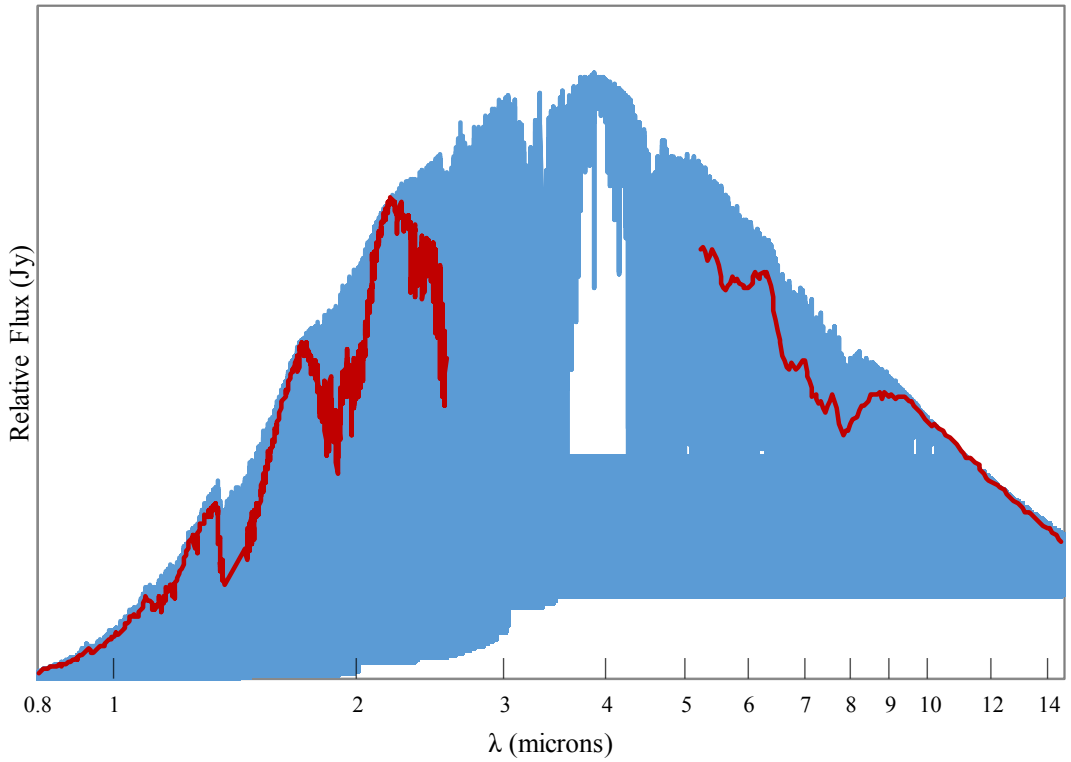

Figure 3.1 Example of a high resolution model (blue) that has been smoothed (red) to the spectral resolution of the extracted spectrum for 2M0559.

resolution of $\Delta\lambda = 1$nm. The resolving power, $R = \lambda/\Delta\lambda$, is the capacity of the spectrometer to resolve two points, which are close together, into individual features. This example spectrometer only allows for R= 20 peaks in the extracted spectrum.

The observed spectra were also a combination of two sources: the reduced mid-infrared Spitzer spectra and published near-infrared spectra. The near-infrared data from 1-2.5μm has a resolving power of $R = 2000 - 10000$, while the extracted data, which spans from 5-15μm, has a power of $R = 60 - 120$ (Esplin 2010). This required a piecewise smoothing function in order to maintain as much spectral detail as possible in the short wavelength. As there were gaps in the short wavelength data, these areas with no spectral data were identified and excluded in the smoothing process (as seen in Figure 3.1 from 2.5-5μm).

3.3 Statistical Fitting Method

A least-squares approach, a form of linear regression, was used to find the best single and binary fit for each brown dwarf. The cost/error functions, G_1 and G_2, in equations (3.1) and (3.2) were used to calculate the best fit for a single and binary system, respectively.

$$G_1 = \sum_i \omega_i (f_i - C' F_i)^2 \tag{3.1}$$

$$G_2 = \sum_i \omega_i (f_i - C' F_i)^2 / C' F_i \tag{3.2}$$

The statistical weighting factor of the ith pixel (ω_i) is the average change in wavelength divided by the mean flux for the original spectrum. The flux values of the models, F_i, represent the values that would be recorded at the surface of star, which is dependent on the radius (R). The flux values of the spectrum as observed from Earth, f_i, are much smaller because the flux of the star decreases with distance (d). Because of this discrepancy in , C' is used as the scale factor, proportional to $(R/d)^2$, that F_i is multiplied with to match the correct order of magnitude of f_i (Esplin 2010).

The equations above were written by Stephens *et al.* (2009), with the smallest returned values for G_1 and G_2 corresponding to the best-fitting models for a single brown dwarf spectrum. Each G_1 value corresponds to a single synthetic model, while G_2 is the result of the addition of two models. If the returned G_2 value is smaller than G_1 for a single star, this indicates that the star is statistically more likely to be a binary system. The returned G values are spectrum-specific and cannot be compared with results from other brown dwarfs. This is because each object spectrum contains a slightly different range of wavelengths, flux values, and number of data points (Stephens et al. 2009).

Chapter 4

Results and Analysis

A single and binary analysis for each potential brown dwarf system was performed by statistically determining which synthetic models best matched the absorption features of the original spectra. Discrepancies between the resulting models and the observed spectrum are explained, and it is concluded that all six brown dwarfs that were analyzed are statistically more likely to be binary systems rather than single stars. The following analysis was also performed on a total of 45 brown dwarfs found in Appendix A.

4.1 Single Fitting Function Results

A single fit was performed using Equation 3.1 in order to determine which models best fit the actual spectrum for each brown dwarf. Each model has a unique combination of four parameters: temperature, surface gravity, cloud density and atmospheric convection. The best single fit parameters for each brown dwarf were recorded in Table 4.1, with the order of the parameters being T_{eff}, log(g), f_{sed}, and K_{zz}. Esplin (2010) returned a best single fit model for 2M0559 of 1200K, log(g)=5, no clouds, and a medium vertical mixing parameter of 2. My best single fit for this object was very similar, but not exact, with 1200K, log(g)=5.5, very thin clouds, and no vertical mixing.

Table 4.1 Best Single Fit Parameters

Name	Temperature	$T_{\rm eff}/log(g)/f_{\rm sed}/K_{\rm zz}$	G_1 Value
Kelu-1	1770-1960K	1700K/5.5/f3/K6	1.78045E-4
2MASSW J0036159+182110	1770K	1800K/5/f3/K0	6.47656E-4
2MASSW J2224438-015852	1650K	1600K/4.5/f1/K4	4.83305E-4
SDSS J080531.83+481233.1	1590K	1700K/5.5/f3/K0	2.62967E-4
SDSS J105213.51+442255.7AB	1220-1450K	1300K/5/f2/K4	1.34678E-4
2MASS J05591914-1404488	1090K	1200K/5.5/f5/K0	2.14685E-4

This slight difference is most likely due to the fact that Esplin did not have access to the improved T dwarf models created by Morley *et al.* (2012) that include Na_2S, KCl, ZnS, MnS, and Cr clouds.

The visual results of the single fitting analysis are shown in Figure 4.1, which compares the best single model to the original spectrum for each star. By visual inspection, it is apparent that the L dwarfs are not well fit from about 8-14μm, as the models curve above the observed spectra. This indicates that red L dwarfs have unique silicate cloud features, and improved cloud models are needed to fully be able to fit all portions of the L dwarf spectrum (Stephens et al. 2009).

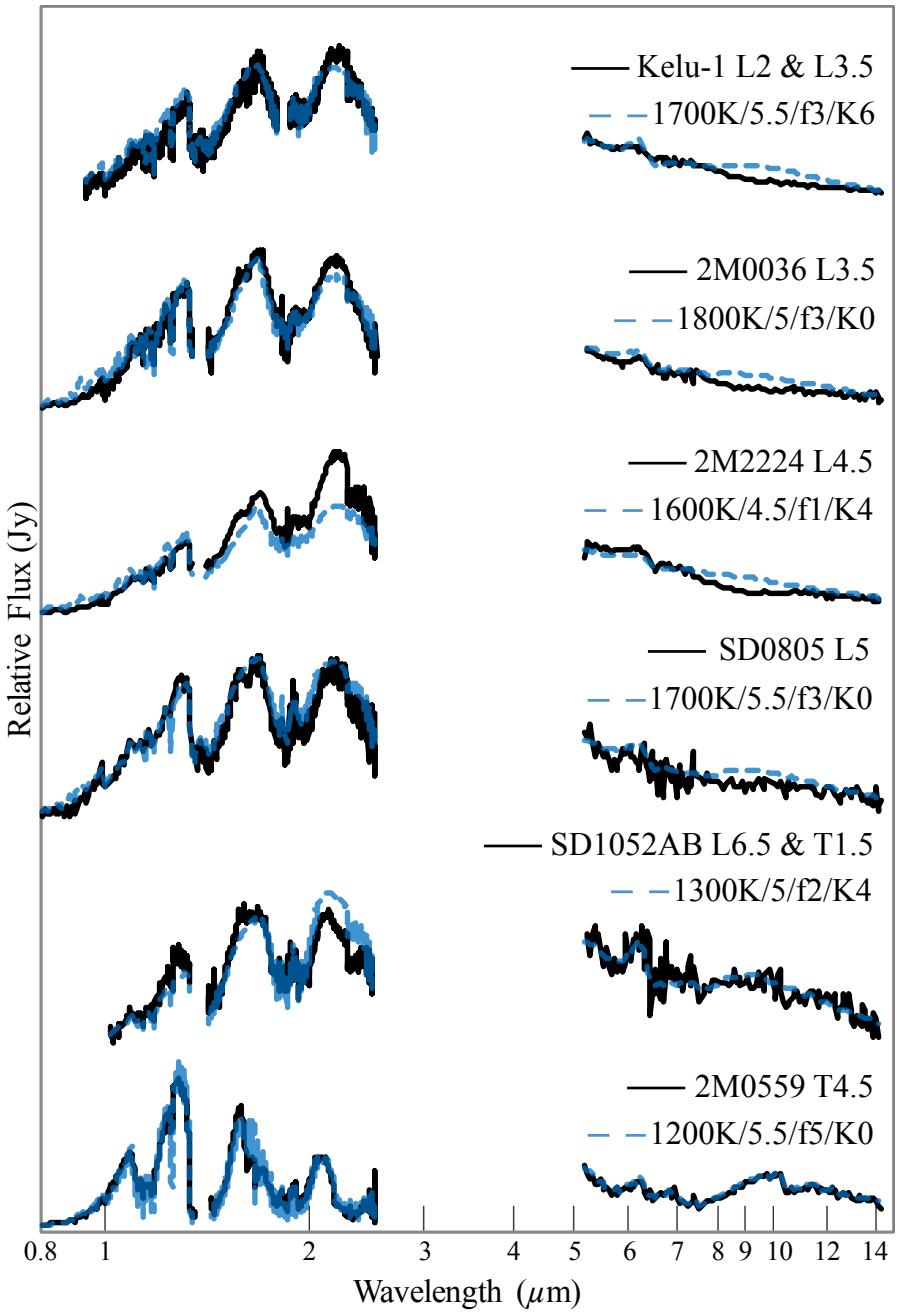

Figure 4.1 The best single models (blue dashed lines) compared to the observed spectra (black lines) for each of the six target brown dwarfs. The parameters T_{eff}/log(g)/f_{sed}/K_{zz} are listed for each model. By visual inspection, the model that best matches the original data corresponds to Kelu-1. However, Kelu-1 is a known binary system, indicating that none of these stars are solitary.

4.2 Binary Fitting Function Results

Each of the six stars analyzed were either suspected or known brown dwarf binary systems. After performing a statistical analysis using Equation 3.2, the best binary fit parameters for each brown dwarf were recorded in Table 4.2, with the order of the parameters again being T_{eff}, log(g), f_{sed} and K_{zz}.

The visual results of the binary fitting analysis are shown in Figure 4.2. Between 1.5-2μm, it is apparent that the models selected for 2M0559, the only dwarf with two possible T dwarf components, do not fit well. This is due to the inability of the model spectra to completely represent the methane absorption features in very cool T dwarfs. When inspecting between 2-2.5μm for each of the other five dwarfs, it is apparent that the models do not fully match the height of the original data, suggesting that the models do not accurately portray the CO band for warm L dwarfs.

Esplin 2010 returned a best binary fit for 2M0559 that was made up of the two following models: 1300K, log(g)=5.5, no clouds, and no vertical mixing combined with 1000K, 4.25 and thin clouds. My best binary fit was similar, but not exact, with 1300K, 5.5, and extremely thin clouds combined with 1000K, 5.5, and medium cloud coverage. While Esplin's exact combination is not among my list of returned best binary fits due to the improved T dwarf models, the temperatures came out the same from both analyses. The statistical fit was significantly better for the binary model in both instances as well, indicating that 2M0559 is likely to be a binary brown dwarf system with the two stars being 1300K and 1000K.

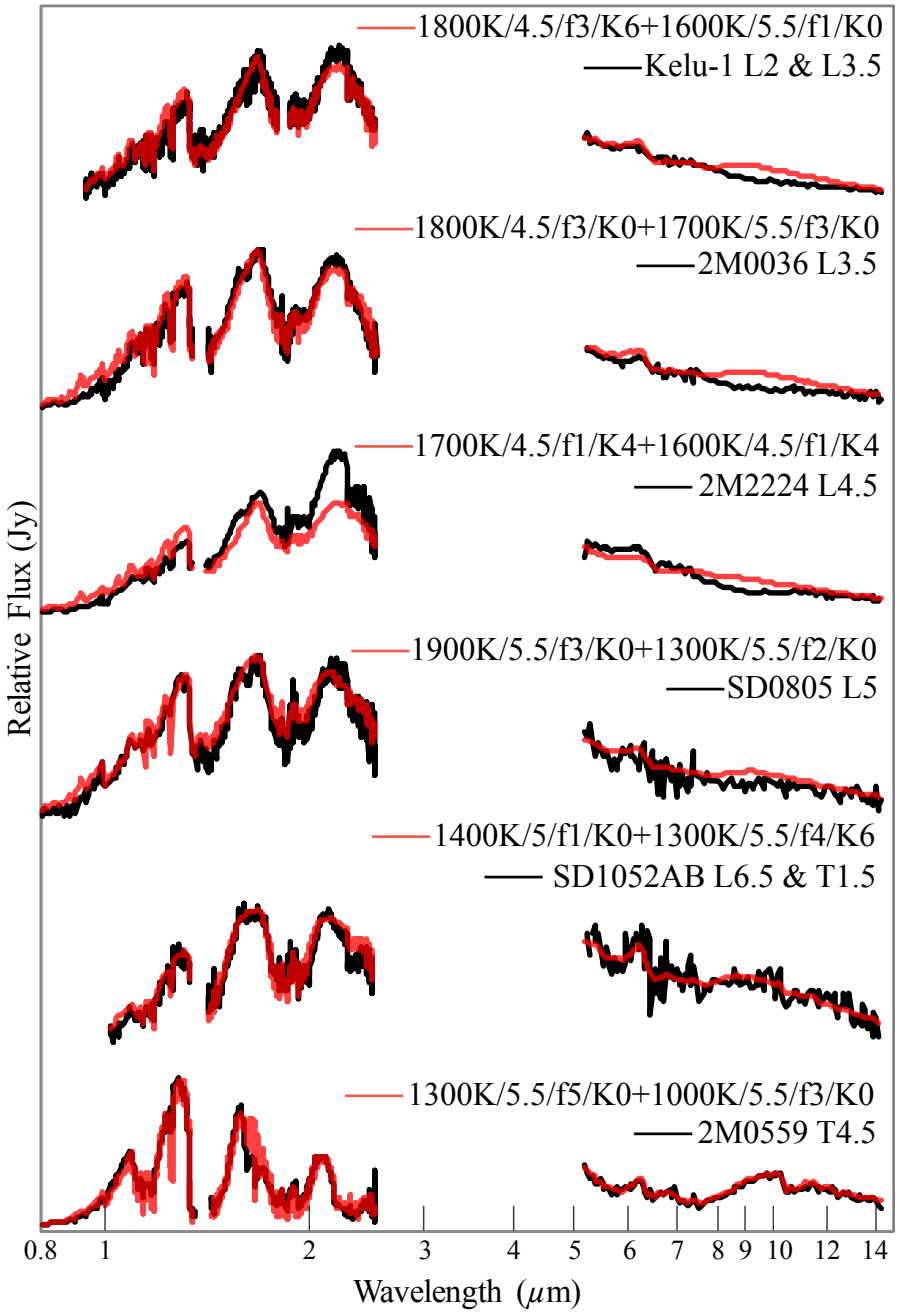

Figure 4.2 The best binary models (red) compared to the observed spectra (black) for each of the six target brown dwarfs. The parameters T_{eff}/log(g)/f_{sed}/K_{zz} are listed for each model.

Table 4.2 Best Binary Fit Parameters

Name	Temperature	$T_{\rm eff}/log(g)/f_{\rm sed}/K_{\rm zz}$	G_2 Value
Kelu-1	1770-1960K	1800K/4.5/f3/K6+1600K/5.5/f1/K0	1.4588E-4
2MASSW J0036159+182110	1770K	1800K/4.5/f3/K0+1700K/5.5/f3/K0	5.59012E-4
2MASSW J2224438-015852	1650K	1700K/4.5/f1/K4+1600K/4.5/f1/K4	4.66623E-4
SDSS J080531.83+481233.1	1590K	1900K/5.5/f3/K0+1300K/5.5/f2/K0	2.48719E-4
SDSS J105213.51+442255.7AB	1220-1450K	1400K/5/f1/K0+1300K/5.5/f4/K6	1.15692E-4
2MASS J05591914-1404488	1090K	1300K/5.5/f5/K0+1000K/5.5/f3/K0	2.09877E-4

4.3 Discussion and Conclusions

A single and binary spectral fitting was performed on the spectral data of four suspected and two known brown dwarf binary systems. Comparing the single model results in Table 4.1 with the binary results in Table 4.2, all six objects returned a smaller G_2, meaning that they were fit best by a binary model. Additionally, a total of 45 brown dwarfs were statistically analyzed and discussed in Appendix A.

The ratio of G_2 to G_1 was calculated to show which stars had the greatest change in fit values. The two known binary systems, Kelu-1 and SD1052, returned the smallest ratios of 0.81934 and 0.85903, while the returned parameters matched very closely to the actual temperature values for each component. SD0805, with the fourth smallest ratio, was identified to potentially be a binary system with L4 (1700K) and T5.5 (1010K) components based on its peculiar spectral features by Burgasser *et al.* (2016). The results of this analysis match their conclusion, as I found the best binary fit of SD0805 to also be an L and T dwarf pair, with respective temperatures of 1900K and 1300K. From these results, I conclude that statistical spectral fitting is a reliable method for estimating the physical parameters of known and potential brown dwarf binary systems.

The best single and binary fits to the original data are visually shown in Figure 4.3. By in-

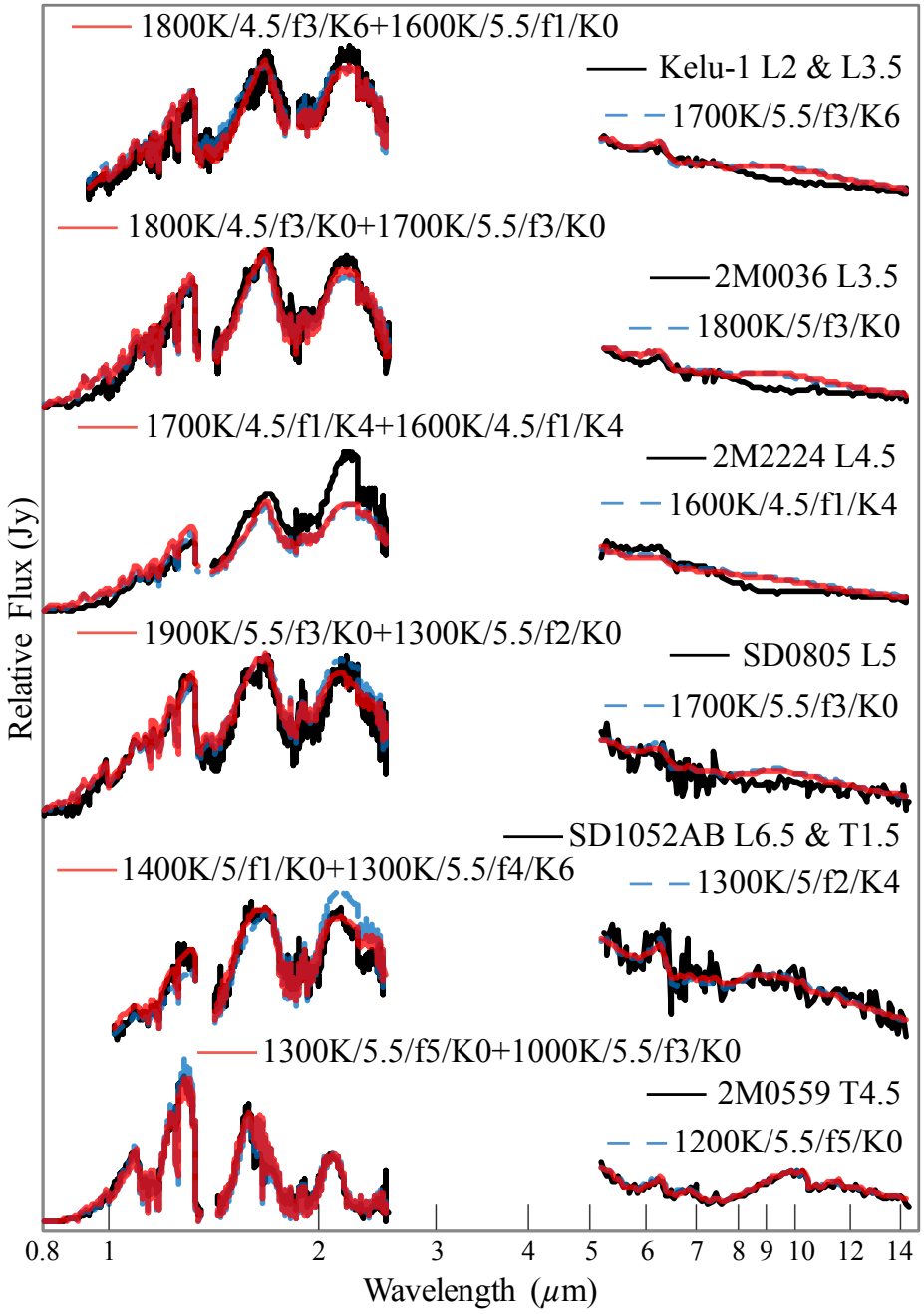

Figure 4.3 The best single (blue) and binary (red) models compared to the observed spectra (black) for each of the six target brown dwarfs. The parameters T_{eff}/log(g)/f_{sed}/K_{zz} are listed for each single and binary model.

spection of this figure, Kelu-1 and 2M0036 fit just slightly better as a binary system. Kelu-1 is a known binary, but the system contains two L dwarfs of similar temperatures. When two objects in a binary system have almost equal temperatures, the spectral features are almost the same. This means that the combined spectrum may appear to be a single star because both components have an almost identical composition. Taking that into consideration, 2M0036 could be either a single brown dwarf with a temperature of 1800K, or a binary system made up of two stars that have a 100K difference.

By inspecting Figure 4.3, it appears that the brown dwarf 2M2224 fits equally well as both a single star and a binary system, with neither being at all close to the original spectrum. 2M2224 is a very red L dwarf, which could be due to a very dusty atmosphere. When dust is present in the atmosphere, the grain sizes are so small that they cannot be accounted for with an $f_{sed} = 1$. The fits to 2M2224 all returned this highest cloud density value, so the best conclusion is that the models are not accurate enough to reproduce a very dusty atmosphere, where the f_{sed} value would fall somewhere between 0 and 1 (Stephens et al. 2009).

SD0805, SD1052, and 2M0559 all fit statistically and visually better as binary systems, and the features of the binary models that do not fit well to the actual data can be easily explained. The weakness of the models from 8-14.5μm is simply due to an inability of the model spectra to accurately portray the silicate cloud features in L dwarfs. The binary model of SD1052 does not perfectly fit from 2-2.5μm as the CO band of L dwarfs cannot fully be reciprocated statistically. Last, 2M0559 is not fit well around 1.6μm as the methane absorption bands in the models also have limitations. Despite these small flaws in the model spectra, SD0805 and 2M0559 are likely to be unequal temperature binary systems.

As brown dwarfs transition from warm L dwarfs to cooler T dwarfs, the clouds thin and decrease in depth until the condensation no longer effects opacity (Stephens et al. 2009). According to Ackerman *et al.* (2001), the cloud density becomes obsolete in the spectral features of stars be-

low 1000K. By inspecting the cloud density parameter for each of the returned fits, it is clear that this trend is followed, as the f_{sed} values tend to increase with decreasing temperature. The most common f_{sed} values for the L dwarfs were 1 and 3, while the returned value for the 1300K component of SD1052 and 2M0559 was 4 and 5 respectively. For both Esplin (2010) and I, the 1000K secondary dwarf in the binary 2M0559 had a relatively high cloud density parameter, suggesting that cloud density begins to increase once stars fall below a certain temperature.

4.4 Future Work

The brown dwarf binary candidates analyzed in this paper were chosen based on results from visual Hubble Space Telescope (HST) images, as the magnitudes indicated a high likelihood of being binary. There are a total of 117 L and T brown dwarfs that have been observed using the Spitzer Infrared Spectrograph, of which only six have now been through the described statistical spectral fitting analysis. The next step will be to obtain visual data from the HST, as many of these brown dwarfs have not yet been observed. Once each of these 117 brown dwarfs have been observed by both Spitzer and Hubble, additional brown dwarf binary candidates can be identified based on the PSF-subtraction technique used on HST images, and a spectral analysis can be performed.

Another future project will be to statistically fit the brown dwarf binary candidates using real brown dwarf spectra as well as models. By fitting data with real rather than synthetic spectra, the discrepancies in the results due to poorly modeled methane, silicate, and other cloud features will be eliminated. This process will show which spectral features are common among L and T dwarfs, as well as which candidates have spectra similar to that of known brown dwarf binaries.

Appendix A

The statistical spectral fitting process described in Chapters 3 and 4 was performed on a total of 45 brown dwarfs with mid and near-infrared spectral data. Additional T dwarf models from Saumon *et al.* (2012) were used. Aside from the six brown dwarfs described in this thesis, the mid-infrared data for the brown dwarfs listed below was obtained from and reduced by the Combined Atlas of Sources with Spitzer IRS Spectra (Lebouteiller et al. 2009). All temperatures shown were provided by Mamajek (2017). Table A.1 is organized by G_2/G_1 values, ranging from smallest (strong binary candidates) to largest (unlikely binary candidates). The order of the best single and binary fit parameters is $T_{\rm eff}/log(g)/f_{\rm sed}/K_{\rm zz}$.

Table A.1 Further Analysis of 45 Brown Dwarfs

Name	Spectral Type	Temperature	Single Fit	Binary Fit	G_2/G_1	Notes
SDSSp J042348.57-041403.5	L7.5	1380K	1400K/5/f2/K2	1400K/4.25/f1/K2+1300K/5.5/f4/K4	0.58684	1,2,3
SDSS J120747.17+024424.8	L8	1350K	1300K/4.25/f2/K2	1400K/4/f1/K4+1200K/5/f4/K0	0.62817	2,4,5
SDSS J075840.32+324723.3	T2	1200K	1100K/4/f2/K2	1200K/5/f4/K4+1000K/5.5/f1/K2	0.69385	2,5
SDSS J125453.90-012247.5	T2	1200K	1200K/4.5/f4/K4	1200K/5.5/f3/K6+1100K/4.5/f2/K0	0.78771	2,6,7
GJ 570D	T7.5	770K	800K/4.5/nc/K6	900K/5/nc/K2+700K/3/nc/K0	0.79545	2,8,9,10
SDSS J111009.99+011613.0	T5.5	1010K	1000K/5/f2/K0	1100K/5/nc/K2+900K/4.5/f1/K2	0.80057	1,2,3,5
2MASSW J1439284+192915	L1	2100K	2200K/4.5/f1/K0	2400K/4.5/nc/K0+1700K/5/f1/K0	0.80882	2,3,5,11
SDSS J151643.00+305344.3	T0.5	1250K	1000K/4/f1/K2	1100K/5.5/f1/K2+1000K/5/f3/K6	0.81270	2,12
2MASSI J0415195-093506	T8	700K	800K/4.5/nc/K4	800K/4/f5/K0+600K/4.5/f3/K2	0.83762	2,5,10,13
2MASSI J0746425+200032	L0.5	2180K	2200K/5/f1/K0	2400K/4.5/f1/K4+2000K/5.5/f1/K4	0.85587	2,3,14,15
SDSS J105213.50+442255.6AB	L6.5 & T1.5	1220-1450K	1300K/5/f2/K4	1400K/5/f1/K0+1300K/5.5/f4/K6	0.85903	12,16,17
Gl 337CD	L8	1350K	1400K/4.75/f2/K0	1500K/4.75/f2/K0+800K/4.25/f2/K0	0.86382	2,18,19
2MASS J08251968+2115521	L7.5	1380K	1300K/4.25/f1/K6	1500K/4.25/f1/K6+1100K/4.25/f1/K6	0.87051	2,3,15,20
2MASSI J0937347+293142C	T6	960K	1000K/5.5/nc/K6	1000K/5.5/nc/K6+600K/5.5/nc/K0	0.88585	2,5,10,13
2MASS J22541892+3123498	T5	1050K	1300K/5/nc/K2	1400K/5.5/nc/K2+1300K/5/f4/K0	0.88800	2,5,8
SDSS J000013.54+255418.6	T4.5	1090K	1300K/5.5/nc/K2	1400K/5.5/nc/K0+600K/4/0.5/K6	0.89250	2,5
SDSS J152039.82+354619.8	T0	1260K	1400K/5/f2/K2	1400K/5/f2/K2+500K/5.3/f0.3/K4	0.89442	2,12
SDSSp J010752.33+004156.1	L8	1350K	1300K/5.5/f2/K0	1300K/5.5/f3/K4+600K/4/0.5/K4	0.90559	1,2,3

2MASS J12255432-2739466	T6	960K	1000K/5/f4/K0	1000K/5.5/f4/K0+950K/3.75/nc/K0	0.91164	1,2,3,21
2MASS J00361617+1821104	L3.5	1770K	1800K/4.5/f2/K0	1900K/4.5/f1/K4+1700K/5.5/f3/K0	0.91346	3,14,15,22
SDSSp J083008.12+482847.4	L9.5	1280K	2000K/4.5/nc/K0	2200K/4.5/nc/K0+800K/4/f2/K0	0.91354	1,2
DENIS-P J025503.3-470049	L9	1300K	1200K/5.5/f3/K6	1200K/4.75/f2/K4+1200K/5.5/f3/K6	0.92293	2,23,24
2MASS J09083803+5032088	L8	1350K	1500K/4.5/f2/K2	1500K/4.5/f2/K2+1500K/5.5/f3/K4	0.92614	2,5,25
SDSSp J162414.37+002915.6	T6	960K	900K/5.5/f3/K6	1000K/5.5/f4/K6+600K/100/f0.5/K4	0.92952	2,26,27
2MASS J05591914-1404488	T4.5	1090K	1200K/5.5/f5/K0	1300K/5.5/nc/K0+1000K/5.5/f5/K0	0.93441	1,3,10,13,22
Gl 584C	L8	1350K	1200K/4.5/f2/K6	1300K/4.75/f2/K2+1000K/5.5/f1/K6	0.93452	2,19,28
Kelu-1	L2 & L3.5	1770-1960K	1800K/5/f1/K0	1900K/4.5/f1/K4+1600K/5.5/f1/K2	0.93515	22,29,30,31
2MASSI J0727182+171001	T7	840K	950K/4.25/nc/K0	900K/4/nc/K2+900K/5.5/nc/K0	0.94295	2,5,10,13
SDSS J085758.44+570851.4	L7	1410K	1400K/4/f1/K0	1400K/4/f1/K2+500K/5.5/nc/K0	0.94493	1,2,3
SDSS J080531.83+481233.1	L5	1590K	1700K/5.5/f3/K0	1900K/5.5/f3/K0+1300K/5.5/f2/K0	0.94582	4,5,12,32
2MASSI J1217110-031113	T7.5	770K	850K/3.75/nc/K0	900K/4.5/f4/K0+800K/3/nc/K0	0.94990	1,2,3,10
SDSS J115553.85+055957.5	L5	1590K	1400K/5.5/f2/K2	1500K/5/f3/K2+1300K/5.5/f1/K0	0.95329	2,5
SDSS J133148.88-011652.5	T0	1260K	1700K/5/f3/K6	1700K/4.5/f4/K6+1500K/4.25/f1/K6	0.95638	2,4,5
2MASS J22244381-0158521	L4.5	1650K	1600K/4.5/f1/K4	1700K/4.5/f1/K4+1600K/4.5/f1/K4	0.96548	1,20,22
2MASSW J0929336+342952	L8	1350K	1200K/4.5/f1/K2	1300K/5.5/f1/K0+650K/5.5/nc/K0	0.97445	2,3,5,20
SDSSp J083717.22-000018.3	T0.5	1250K	1100K/5.5/f3/K6	1200K/5/f3/K6+800K/3/nc/K0	0.97702	2,6,11
2MASS J05395200-0059019	L5	1590K	1800K/4.5/f1/K0	1800K/4.5/f1/K6+1800K/5/f3/K0	0.98109	1,2,3,33
2MASS J12095613-1004008	T2 & T7.5	770-1200K	2100K/5.5/nc/K0	2400K/5.5/nc/K0+1300K/5/nc/K0	0.98194	2,12,34,35
SDSS J102109.69-030420.1	T1 & T4	1120-1230K	1800K/5.5/nc/K0	2000K/5.5/nc/K0+900K/3/nc/K0	0.98546	1,2,6,36

2MASSW J1658037+702701	L1	2100K	2400K/4.5/f1/K0	2400K/4.5/f1/K0+400K/4/f2/K0	0.99228	2,19,37
Gl 229B	T6.5	900K	1000K/5.5/f1/K4	1000K/5.5/f1/K4+1000K/5.5/f1/K2	0.99942	2,38,39
2MASS J15074769-1627386	L5	1590K	1700K/5.5/f3/K6	1700K/5.5/f3/K6+1700K/5.5/f3/K6	1	2,3,5,14,40
GJ 1001B	L5 & L5	1590K	1100K/5.5/f1/K6	1100K/5.5/f1/K6+1100K/5.5/f1/K6	1	2,3,23,41,42
2MASS J22443167+2043433	L6.5	1450K	1300K/5.5/f1/K6	1300K/5.5/f1/K6+1300K/5.5/f1/K6	1	2,5,43
DENIS-P J1228.2-1547	L5	1590K	2400K/5/nc/K0	2400K/5/nc/K0+2400K/5/nc/K0	1	2,11,23,30,44

Note. – (1) Near-infrared data provided Geballe *et al.* (2002); (2) mid-infrared data provided by Lebouteiller *et al.* (2011); (3) near-infrared data provided by Leggett *et al.* (2002); (4) discovery by Hawley *et al.* (2002); (5) contributions made by Knapp *et al.* (2004); (6) contributions made by Leggett *et al.* (2000); (7) near-infrared data provided by Rayner *et al.* (2009); (8) discovery by Burgasser *et al.* (2000b); (9) near-infrared data provided by Geballe *et al.* (2001); (10) contributions made by Burgasser *et al.* (2003); (11) discovered by Kirkpatrick *et al.* (1999); (12) contributions made by by Chiu *et al.* (2006); (13) discovery by Burgasser *et al.* (2002); (14) discovery by Reid *et al.* (2000); (15) near-infrared data provided by Reid *et al.* (2001); (16) mid-infrared data requested by David Golimowski in 2006 (Program ID 20514); (17) resolved L and T binary by Dupuy *et al.* (2015); (18) discovery by Wilson *et al.* (2001); (19) near-infrared data provided by McLean *et al.* (2003); (20) contributions made by Kirkpatrick *et al.* (2000); (21) discovery by Burgasser *et al.* (1999); (22) mid-infrared data requested by Houck *et al.* (2004); (23) discovery by Martin *et al.* (1999); (24) near-infrared data provided by Cushing *et al.* (2005); (25) contributions made by Cruz *et al.* (2003); (26) contributions made by Strauss *et al.* (1999); (27) near-infrared data provided by Bergasser *et al.* (2000a); (28) discovery by Kirkpatrick *et al.* (2001); (29) contributions made by Ruiz *et al.* (1997); (30) near-infrared data provided by Leggett *et al.* (2001); (31) resolved binary by Liu and Leggett (2005); (32) mid-infrared data requested by Sandy Leggett in 2004 (Program ID 3431); (33) contributions made by Fan *et al.* (2000); (34) discovery by Burgasser *et al.* (2004); (35) binary parameters given by Liu *et al.* (2010); (36) binary parameters given by Gelino *et al.* (2014); (37) discovery by Gizis *et al.* (2000); (38) discovery

by Nakajima *et al.* (1995); (39) near-infrared data provided by Golimowski *et al.* (2004); (40) near-infrared data provided by Noll *et al.* (2000); (41) discovery by Goldman *et al.* (1999); (42) binary parameters given by Reid *et al.* (2008); (43) discovery by Dahn *et al.* (2002); (44) near-infrared data provided by Tinney *et al.* (1998).

Bibliography

Ackerman, A. S., & Marley, M. S. 2001, The Astrophysical Journal, 556, 872

Burgasser, A. J. 2003 (United States: USDOE Office of Science (SC))

Burgasser, A. J., Blake, C. H., Gelino, C. R., Sahlmann, J., & Gagliuffi, D. B. 2016, The Astrophysical Journal, 827, 25

Burgasser, A. J., McElwain, M. W., Kirkpatrick, J. D., Cruz, K. L., Tinney, C. G., & Reid, I. N. 2004, The Astronomical Journal, 127, 2856

Burgasser, A. J., et al. 1999, The Astrophysical Journal Letters, 522, L65

—. 2000a, The Astronomical Journal, 120, 1100

—. 2000b, The Astrophysical Journal Letters, 531, L57

—. 2002, The Astrophysical Journal, 564, 421

—. 2006, The Astrophysical Journal, 637, 1067

Chiu, K., Fan, X., Leggett, S. K., Golimowski, D. A., Zheng, W., Geballe, T. R., Schneider, D. P., & Brinkmann, J. 2006, The Astronomical Journal, 131, 2722

Cooper, C. S., Sudarsky, D., Milsom, J. A., Lunine, J. I., & Burrows, A. 2003, The Astrophysical Journal, 586, 1320

Cruz, K. L., Reid, I. N., Liebert, J., Kirkpatrick, J. D., & Lowrance, P. J. 2003, The Astronomical Journal, 126, 2421

Cushing, M. C., Rayner, J. T., & Vacca, W. D. 2005, The Astrophysical Journal, 623, 1115

Dahn, C. C., et al. 2002, The Astronomical Journal, 124, 1170

Dupuy, T., Liu, M. C., Leggett, S. K., Ireland, M., Chiu, K., & Golimowski, D. A. 2015

Dyk, S. V., Werner, M., & Silbermann, N. 2013, Spitzer Telescope Handbook

Esplin, T. 2010, Statistical Spectral Fitting of the Brown Dwarf Binary System 2M0559, Bachelors Thesis (Brigham Young University)

Fan, X., et al. 2000, The Astronomical Journal, 119, 928

Geballe, T. R., Saumon, D., Leggett, S. K., Knapp, G. R., Marley, M. S., & Lodders, K. 2001, The Astrophysical Journal, 556, 373

Geballe, T. R., et al. 2002, The Astrophysical Journal, 564, 466

Gelino, C. R., et al. 2014, The Astronomical Journal, 148, 6

Gizis, J. E., Monet, D. G., Reid, I. N., Kirkpatrick, J. D., Liebert, J., & Williams, R. J. 2000, The Astronomical Journal, 120, 1085

Goldman, B., Delfosse, X., Forveille, T., & collaboration, C. A. e. a. t. E. 1999

Golimowski, D. A., et al. 2004, The Astronomical Journal, 127, 3516

Hawley, S. L., et al. 2002, The Astronomical Journal, 123, 3409

Higdon, S. J. U., et al. 2004, Publications of the Astronomical Society of the Pacific, 116, 975

Houck, J. R., et al. 2004, The Astrophysical Journal Supplement Series, 154, 18

Kirkpatrick, J., et al. 1999

Kirkpatrick, J. D., Dahn, C. C., Monet, D. G., Reid, I. N., Gizis, J. E., Liebert, J., & Burgasser, A. J. 2001, The Astronomical Journal, 121, 3235

Kirkpatrick, J. D., et al. 2000, The Astronomical Journal, 120, 447

Knapp, G. R., et al. 2004, The Astronomical Journal, 127, 3553

Krist, J., & Hook, R. 2004, The Tiny Tim User's Guide

Lebouteiller, V., Barry, D. J., Spoon, H. W. W., Bernard-Salas, J., Sloan, G. C., Houck, J. R., & Weedman, D. W. 2011

Lebouteiller, V., Bernard-Salas, J., Sloan, G. C., & Barry, D. J. 2009

Leggett, S. K., Allard, F., Geballe, T. R., Hauschildt, P. H., & Schweitzer, A. 2001, The Astrophysical Journal, 548, 908

Leggett, S. K., Geballe, T. R., & Fan, X. 2000

Leggett, S. K., et al. 2002, The Astrophysical Journal, 564, 452

Liu, M. C., Dupuy, T. J., & Leggett, S. K. 2010, The Astrophysical Journal, 722, 311

Liu, M. C., & Leggett, S. K. 2005, The Astrophysical Journal, 634, 616

Mamajek, E. 2017, A Modern Mean Dwarf Stellar Color and Effective Temperature Sequence

Martín, E. L., Delfosse, X., Basri, G., Goldman, B., Forveille, T., & Osorio, M. R. Z. 1999, The Astronomical Journal, 118, 2466

McLean, I. S., McGovern, M. R., Burgasser, A. J., Kirkpatrick, J. D., Prato, L., & Kim, S. S. 2003, The Astrophysical Journal, 596, 561

Morley, C. V., Fortney, J. J., Marley, M. S., Visscher, C., Saumon, D., & Leggett, S. K. 2012

Nakajima, T., Kulkarni, S. R., Golimowski, D. A., Durrance, S. T., Matthews, K., & Oppenheimer, B. R. 1995, Nature, 378, 463

Noll, K. S., Geballe, T. R., Leggett, S. K., & Marley, M. S. 2000, The Astrophysical Journal Letters, 541, L75

Rayner, J. T., Cushing, M. C., & Vacca, W. D. 2009, The Astrophysical Journal Supplement Series, 185, 289

Reid, I. N., Burgasser, A. J., Cruz, K. L., Kirkpatrick, J. D., & Gizis, J. E. 2001, The Astronomical Journal, 121, 1710

Reid, I. N., Cruz, K. L., Kirkpatrick, J. D., Allen, P. R., Mungall, F., Liebert, J., Lowrance, P., & Sweet, A. 2008, The Astronomical Journal, 136, 1290

Reid, I. N., Kirkpatrick, J. D., Gizis, J. E., Dahn, C. C., Monet, D. G., Williams, R. J., Liebert, J., & Burgasser, A. J. 2000, The Astronomical Journal, 119, 369

Ruiz, M. T., Leggett, S. K., & Allard, F. 1997, The Astrophysical Journal Letters, 491, L107

Saumon, D., & Marley, M. S. 2008, The Astrophysical Journal, 689, 1327

Saumon, D., Marley, M. S., Abel, M., Frommhold, L., & Freedman, R. S. 2012

Stephens, D. C., et al. 2009, The 0.8 to 14.5 m Spectral Energy Distributions of Mid-L to Mid-T Dwarfs.

Strauss, M. A., et al. 1999, The Astrophysical Journal Letters, 522, L61

Tinney, C. G., Delfosse, X., Forveille, T., & Allard, F. 1998

Tody, D. 1986, Proc. SPIE Instrumentation in Astronomy VI, ed. D.L. Crawford, 627, 733

Werner, M. W., et al. 2004, The Astrophysical Journal Supplement Series, 154, 1

Wilson, J. C., Kirkpatrick, J. D., Gizis, J. E., Skrutskie, M. F., Monet, D. G., & Houck, J. R. 2001, The Astronomical Journal, 122, 1989

Index